STRUCTURED MULTIBLOCK FLOW SIMULATIONS OVER SOUNDING ROCKET CONFIGURATIONS INCLUDING THE INFLUENCE OF FINS

José Carlos Papa
Instituto de Aeronáutica e Espaço
Centro Técnico Aeroespacial
CTA/IAE/ASB
12228-904 – São José dos Campos –SP – BRAZIL
jcpmba@bol.com.br

João Luiz F. Azevedo
Instituto de Aeronáutica e Espaço
Centro Técnico Aeroespacial
CTA/IAE/ASE-N
12228-904 – São José dos Campos –SP – BRAZIL
azevedo@iae.cta.br

Abstract. *Aerodynamic flow simulations over a typical sounding rocket are presented. Sounding rocket configurations usually require fairly large fins and, quite frequently, have more than one set of fins. In order to be able to handle such configurations, the present work uses a novel methodology which combines both Chimera and patched multiblock grids in the discretization of the computational domain. The flows of interest are modeled using the 3-D Euler equations and the work decribes the details of the discretization procedure, which uses a finite difference approach for structured, body-conforming, multiblock grids. The method is used to calculate the aerodynamics of a sounding vehicle currently under development. The results indicate that the present approach can be a powerful aerodynamic analysis and design tool.*

Keywords*. aerodynamic flow simulations, sounding rocket, fins, multiblock grids.*

1. Introduction

In the present work, the results obtained for the simulation of aerodynamic flow about a typical sounding rocket, the SONDA-III, are presented. This work is inserted in the effort of developing the computational tools necessary to simulate aerodynamics flows on aerospace geometries, especially those related to the Brazilian Satellite Launcher VLS (Azevedo *et al.*, 1995; Azevedo *et al.*, 1996; Azevedo *et al.*, 1997; Strauss *et al.*, 1999) and the SONDA-III. The SONDA-III presents a quite complex geometric configuration with four front fins and four back fins around a central core. The fins are arranged symmetrically around the central body. An illustrative outline of this configuration is presented in Fig. (1). Therefore, mesh generation for the flow simulation can be a very labourious process either with structured or unstructured grid technologies. The region shown in Fig. (2) is the most complex to generate quality meshes. The fins possess a reasonable thickness, even at the trailing adge. The reseach group has a fair amount of experience with Chimera and patched multiblock flow simulations for launch vehicle simulations. But this is the first time that the group uses the two techniques in the same code. This is also the first time that the group simulates a vehicle with fins. The initial objective of the present effort is, therefore, to demonstrate that the use of the two techniques combined will enable the generation of better quality grids for the problems at hand.

The code for the simulation of the flow over the SONDA-III with Chimera and patched multiblock aproach was obtained as a continuation of the development of the code already available for Chimera grid simulations for the VLS (Basso *et al.*, 2000), which had already been validated.

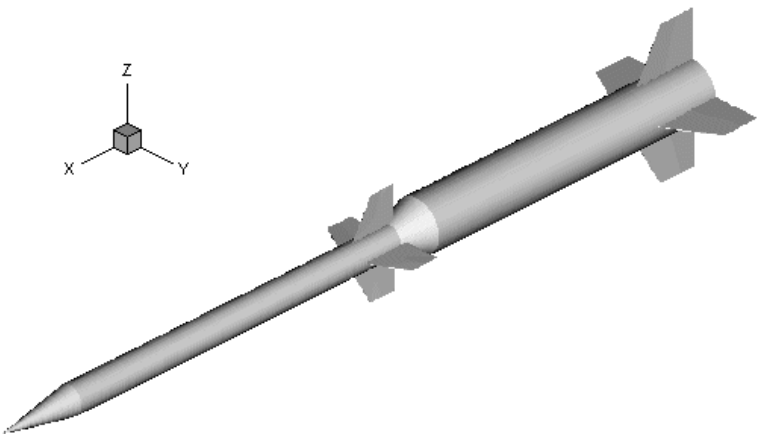

Figure 1. Perspective view of the SONDA-III.

The governing equations are assumed written in conservative form and the equations are discretized in a finite difference context. Spatial discretization uses second-order accurate, central difference operators. The time march method is based on a 5-stage, Runge-Kutta algorithm (Jameson *et al.*, 1981; Jameson *et al.*, 1986), which also has second-order accuracy in time. The artificial dissipation terms added are based on non-isotropic, Turkel and Vatsa model (Turkel *et al.*, 1994).

In the present case, Chimera and patched grid techniques are used to simulate flows over the complete SONDA-III rocket. Those techniques together provide the capability to use structured meshes for the discretization of the calculation domain over truly complex configurations. Moreover, they allow grid refinement characteristics which are similar to those achieved with unstructured meshes. The paper will briefly describe the theoretical formulation used together with a discussion of the numerical implementation aspects and boundary conditions adopted. Details of the current implementation of the Chimera and patched grid techniques are also presented. Results with applicattions to the SONDA-III are described and some concluding remarks are presented.

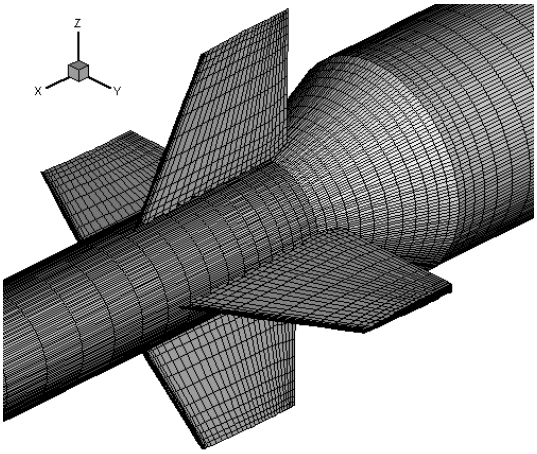

Figure 2. Detail of the front fin region.

2 Theoretical Formulation

It is assumed that the flows of interest in the present work can be represented by the Euler equations in three dimensions. These equations can be written in conservative-law form for a curvilinear coordinate system as

$$\frac{\partial \overline{Q}}{\partial \tau}+\frac{\partial \overline{E}}{\partial \xi}+\frac{\partial \overline{F}}{\partial \eta}+\frac{\partial \overline{G}}{\partial \zeta}=0\,, \tag{1}$$

where $\overline{Q}$ is the vector of conserved variables, defined as

$$\overline{Q}=J^{-1}\left[\rho,\rho u,\rho v,\rho w,e\right]^{T}. \tag{2}$$

In the equations, ρ is the density, *u,v,w* are the Cartesian velocity components and *e* is the total energy per unit of volume. The $\overline{E}$, $\overline{F}$ and $\overline{G}$ are the inviscid flux vectors, *J* is the Jacobian of the transformation, represented as

$$J=\left(x_\xi y_\eta z_\varsigma+x_\eta y_\varsigma z_\xi+x_\varsigma y_\xi z_\eta-x_\xi y_\varsigma z_\eta-x_\eta y_\xi z_\eta-x_\varsigma y_\eta z_\xi\right)^{-1}. \tag{3}$$

Expressions for the inviscid flux vectors can be found in Vieira *et al.* (1998), among other references. The pressure can be obtained from the equation of state for a perfect gas as

$$p=(\gamma-1)\left[e-\frac{1}{2}\rho\left(u^2+v^2+w^2\right)\right]. \tag{4}$$

A suitable nondimensionalization of the governing equations has been assumed in order to write Eq. (1). In particular, the values of flow properties are made dimensionless with respect to freestream quantities, as described in Pulliam *et al.* (1980).

The governing equations were discretized in a finite difference context in structured hexahedral meshes which would conform to the bodies in the computacional domain. Since a central difference spatial discretization method is being used, artificial dissipation terms must be added to the formulation in order to control nonlinear instabilities. The artificial dissipation terms used here are based on Turkel and Vatsa's scalar model (Turkel *et al.*, 1994). This model is nonlinear and non-isotropic, with the scaling of the artificial dissipation operator in each coordinate direction weighted by its own spectral radius of the corresponding flux Jacobian matrix. In the present implementation, the residue operator is defined as

$$RHS^n = -\Delta t\left(\delta_\xi E^n + \delta_\mu F^n + \delta_\varsigma G^n\right). \tag{5}$$

Here, the δ_ξ, δ_η and δ_ς terms represent mid-point central difference operators in the ξ, η and ς directions, respectively. The numerical flux vectors are defined as

$$\begin{aligned} E_{i\pm1/2,j,k} &= \frac{1}{2}\left(\overline{E}_{i,j,k} + \overline{E}_{i\pm1,j,k}\right) - d_{i\pm1/2,j,k}, \\ F_{i,j\pm1/2,k} &= \frac{1}{2}\left(\overline{F}_{i,j,k} + \overline{F}_{i,j\pm1,k}\right) - d_{i,j\pm1/2,k}, \\ G_{i,j,k\pm1/2} &= \frac{1}{2}\left(\overline{G}_{i,j,k} + \overline{G}_{i,j,k\pm1}\right) - d_{i,j,k\pm1/2}. \end{aligned} \tag{6}$$

The artificial dissipation operators, $d_{i\pm1/2,j,k}$, $d_{i,j\pm1/2,k}$ and $d_{i,j,k\pm1/2}$, are defined precisely as described in Turkel *et al.* (1994).

Since steady state solutions were the major interest in present study, a variable time step convergence acceleration procedure has been implemented. In the present case, the time step is defined as

$$\Delta t_{i,j,k} = \frac{CFL}{c_{i,j,k}}. \tag{7}$$

The characteristic velocity $c_{i,j,k}$ is defined as

$$c_{i,j,k} = \max\left(|U| + a\sqrt{\xi_x^2 + \xi_y^2 + \xi_z^2}, |V| + a\sqrt{\eta_x^2 + \eta_y^2 + \eta_z^2}, |W| + a\sqrt{\varsigma_x^2 + \varsigma_y^2 + \varsigma_z^2}\right)_{i,j,k}, \tag{8}$$

where *a* is the speed of sound and *U*, *V* and *W* are the contravariant velocity components.

The time march is performed based on a 5-stage, 2nd-order accurate, hybrid Runge-Kutta time-stepping scheme, where

$$\begin{aligned} &\overline{Q}_i^{(0)} = \overline{Q}_i^n \\ &\overline{Q}_i^{(l)} = \overline{Q}_i^{(0)} - \alpha_l RHS^{(l-1)}, \qquad \text{where } \alpha_1 = 1/4,\ \alpha_2 = 1/6,\ \alpha_3 = 3/8,\ \alpha_4 = 1/2 \text{ e } \alpha_5 = 1, \\ &\overline{Q}_i^{n+1} = \overline{Q}_i^{(5)}, \end{aligned} \tag{9}$$

It should be emphasized that only the convective operator inside the RHS term indicated in Eq. (9) is actually evaluated at every time step. The artificial dissipation term is only evaluated in the first and second stages of the time-march procedure. It can be shown that this provides enough damping to mantain nonlinear stability (Jameson *et al.*, 1981) whereas it yields a more efficient numerical scheme.

3 Computacional Grid Topology

The SONDA-III rocket possesses a central body where four front fins and four back fins are mounted. In order to save computacional resources, 1/8 of the complete configuration in the azimutal direction was simulated. This simplification is valid in the present work because only simulations with zero attack angle were considered. This way, taking advantage the symmetry of the problem, the configuration is reduced to 1/8 of the central body in the azimutal direction, 1/2 front fin, and 1/2 back fin. In total, 13 meshes with relatively simple geometry to model the rocket and the fins were used. These meshes are distributed in the following way:

- 7 meshes for the front fin, denominated $m_1, m_2, m_3, m_4, m_5, m_6$ e m_7, Fig.(3);
- 3 meshes for the back fin, denominated m_9, m_{10} e m_{11}, Fig. (4);
- 1 mesh for the central body, denominated m_{13}, Fig. (5);
- 1 "background" mesh for front fin, denominated m_8, Fig. (5);
- 1 "background" mesh for back fin, denominated m_{12}, Fig. (5).

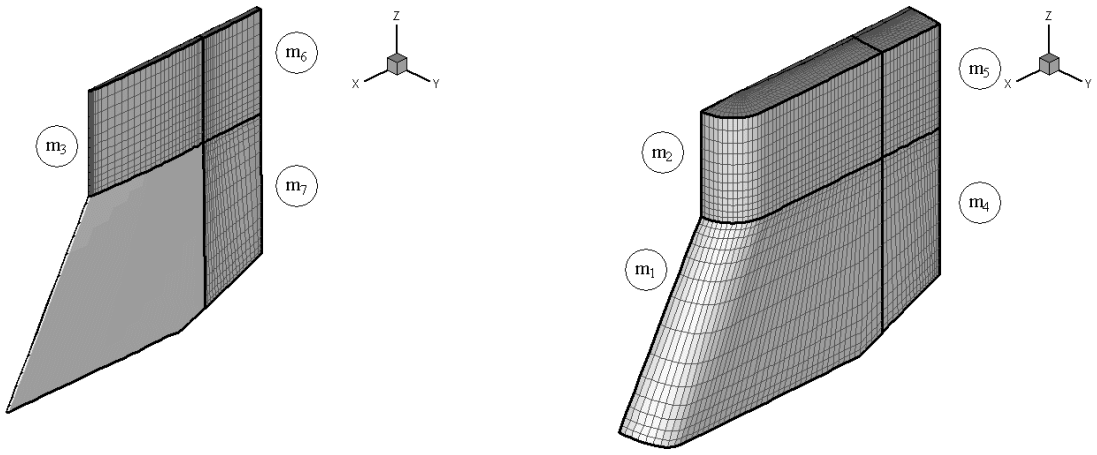

Figure 3. Front fin meshes.

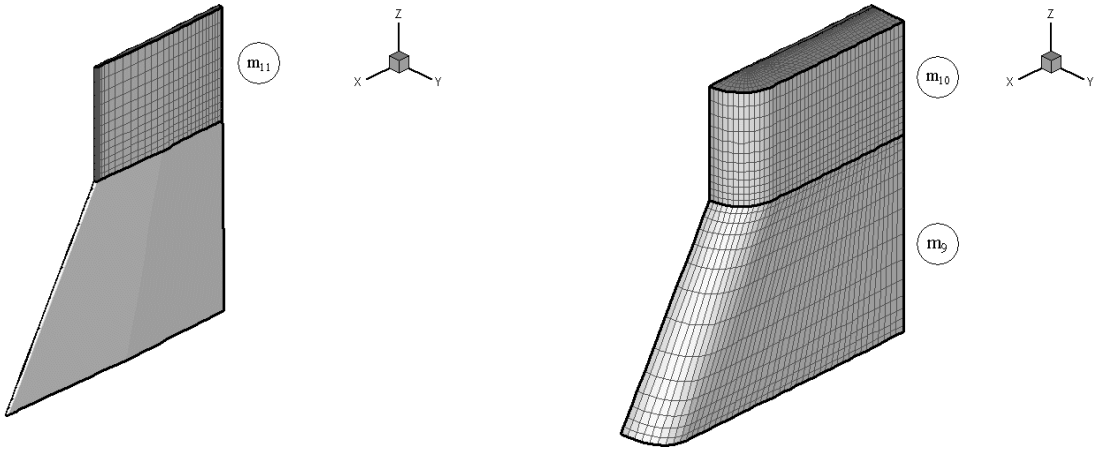

Figure 4. Back fin meshes.

The computational meshes used in the present work were all generated by algebraic methods within each block. In particular, the multisurface algebraic grid generation technique described by Fletcher (1988) has been implemented in a fairly general code for the present configurations. The code allows grid clustering at various regions and a fair amount of control on the grid point distribuition along the normal direction. Both hyperbolic tangent and exponential grid stretching functions are used to obtain the desired grid clustering and coarsening over the body. The meshes generated by that method are 2-D. The mesh that discretizes the central body is rotated around the longitudinal axis, obtaining a 3-D mesh. Initially, for the fins, 2-D meshes are generated for the superior and inferior surface. The inferior surface is deformed through a mathematical transformation to conform to the cylindrical and conical sections of the central body. Finally, intermediate surfaces are obtained through an interpolation of the superior and inferior surfaces previously calculated (Fig. (6)).

The code for the VLS used only Chimera grids. However, during the initial mesh planning phase for SONDA-III, the study group noticed that, due to the geometric characteristics of the new problem, using only Chimera meshes would not be viable. The adopted solution was to use Chimera in conjunction with patched grids. This procedure made possible to generate the meshes in a much simpler way, in comparison with other proposals that just used one technique or another. The Chimera subroutines of the original solver for the VLS were adapted and it was implemented additional subroutines for the use of patched grids. It was also implemented routines for the control of the flow of information among the meshes, and all the particularities of the original code for the configuration of the VLS were eliminated. With that, the study group developed a somewhat general code, that can work with Chimera and patched grids, in

complex configurations. The number of meshes that the code can manage is just limited by the amount of memory of the machine.

The flow of information among the meshes can be seen in Fig. (7). Basically, the m_1 to m_7 meshes, that involve the front fin, change information amongst themselves using the technique of patched meshes. These 7 meshes change information with the m_8 mesh (one of the two "background" meshes), and finally, the m_8 mesh changes information with the central body mesh, m_{13}. For the back fins, the process is similar. The "background" mesh has the function of serving as transition among the fin meshes (that possesses a large number of points) and the central body mesh (that possesses few points). Besides, the background mesh hides the complexity of the configuration, since the central body mesh does not see the fin meshes. In case the "background" meshes were not used, the central body mesh would need to have a lot more points in order to communicate in an efficient way with the fin meshes.

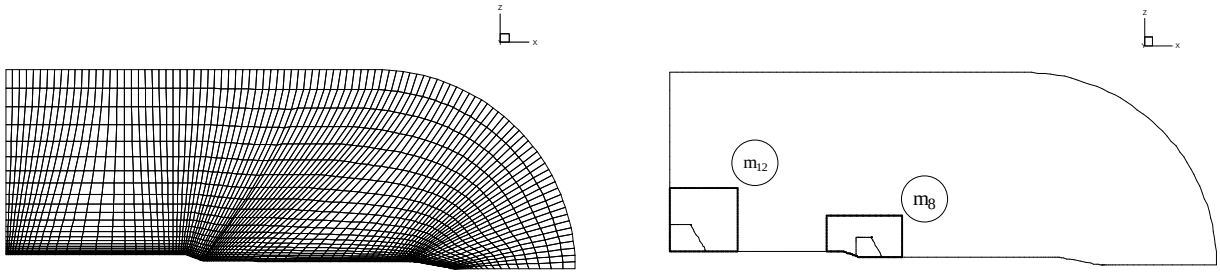

Figure 5. Central body mesh (left), m_{13}, and the background meshes (right), m_8 and m_{12}.

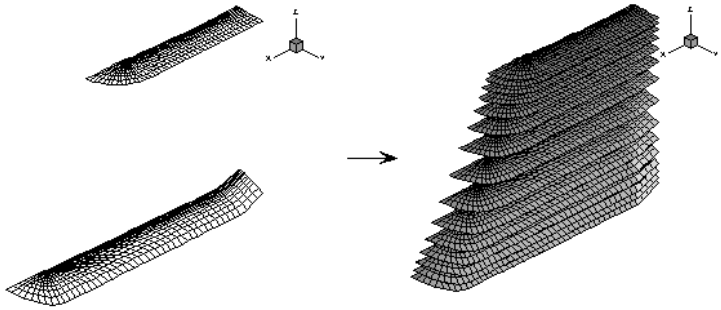

Figure 6. Intermediate surfaces obtained by interpolation of the tip and root surfaces of the front fin.

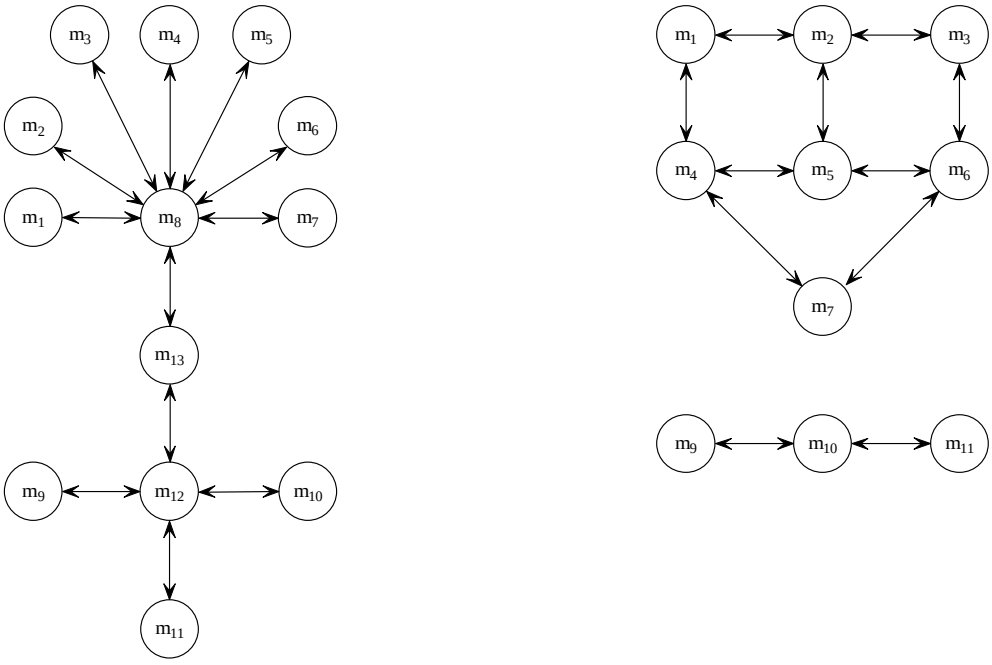

Figure 7. Information flow of the Chimera meshes (left) and of the patched meshes (right).

5 Treatment of Patched Grid Interfaces

In this present work, a patched grid always shares a common face of points with other patched grid mesh. As it will be explained ahead, those meshes should be modified and that modification has the effect of increasing the common point area. To illustrate this procedure, we will suppose that we have two meshes, denominated *A* and *B*, as presented in the left side of Fig. (8). Those meshes should be expanded, in order to make possible the implementation of a code with the capacity to transfer information through the common faces. It is desirable to maintain the order of the artificial dissipation in all points. Taken into account that the artificial dissipation uses 5 points, a possible solution is to expand the meshes so that there is an area of 5 rows of points in common, as indicated in the right side of Fig. (8). It can be observed that 2 rows of points were added to each mesh, which caused the displacement of the first column of points. The following steps are executed:

- Initially, the properties of all interior points located in the expanded *A* mesh are calculed, advancing one step in time.
- The points located in the first column of the *B* mesh receive the values of the properties of the points of the fifth column of the *A* mesh.
- The points located in the second column of the *B* mesh receive the values of the properties of the points of the fourth column of the *A* mesh.
- All the interior points of the *B* mesh are calculed, advancing one step in time for that mesh.
- The values of the points located in the fifth column of the *B* mesh are transferred for the first column of the *A* mesh, and the values of the fourth column of the *B* mesh for the second column of the *A* mesh.
- The interior points of the *A* mesh are calculed again and the process repeats itself.

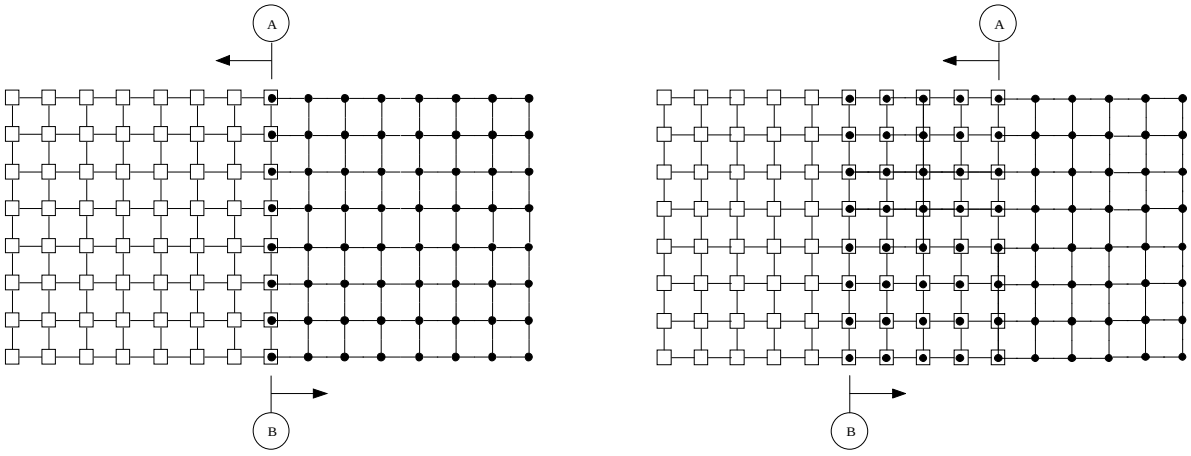

Figure 8. *A* and *B* meshes before (left) and after (right) the expansion process.

The third column of the two meshes is left "free" and its value is determined by the calculation of the interior points, without any imposition of values, as it happened with the first and the second columns. Attempts of imposing some value in the third column, as for exemple an average among the two meshes, resulted in a significant decrease of the convergence rate. In 3-D, instead of lines or columns, the meshes have planes in common. In the present work, the meshes are built with a single face in common, and an additional code takes charge of reading a connection matrix (represented graphically in the right side of Fig. (7)) to decide which faces of each mesh should be expanded. An interesting fact to be observed is when there are 3 meshes in "L" around a wall, as it happens with the meshes m_3, m_6 and m_7 in the Fig. (3), a volume of points without physical sense is created in the middle mesh. The code should be capable of identifying those volumes and of ignoring them.

6 The Chimera Holecutting Process

The Chimera grid possesses a sobreposition area, but unlike the patched grid, there is no need for the points to coincide. Again, that area is responsible for the exchange of information among the meshes. However, as not all of the points are necessary for the communication among the meshes, we can logically eliminate some points. Actually, all of the points continue to exist in the computer memory. We create an auxiliary matrix that associates to each point of the mesh an "on value" or an "off value". The points are eliminated by two reasons. The first one concerns the fact that points of a certain mesh are located inside an area without physical sense of another mesh, as a solid area. An example would be the points of the m_8 mesh that are located inside the front fin. The left side of Fig. (9) exhibits the mesh m_8 with the points eliminated, and the outline of the fin. In practice, a virtual volume larger than the solid volume is

created, and all points of the mesh that are inside the virtual volume are eliminated. The creation of the virtual volume makes possible the control of the amount of points to be eliminated. The second reason for eliminating points is to reduce the sobreposition area. An example would be the central body mesh m_{13}, that contains the two "background" meshes m_8 and m_{12}. A virtual volume completely contained in a "background" mesh is created and all points of the mesh that are inside this volume are eliminated. The right side of Fig. (9) displays the result of this process.

After the "holecutting" process, the next step consists in identifying the Chimera boundary points. These points are the ones that were not eliminated by the previous process, but that possess at least a neighbor that was eliminated. The Chimera boundary points are not calculated in the same way that the other interior points. They have the values of their properties interpolated. Each Chimera boundary point is located inside of a hexahedron whose vertices are formed by points of the other Chimera grid. We will call p_1, p_2, p_3, p_4, p_5, p_6, p_7 and p_8 the distances between a Chimera boundary point of the first mesh and each of the eight vertices of the second mesh, respectively. The following values are calculated

$$
\begin{aligned}
H_1 &= p_2.p_3.p_4.p_5.p_6.p_7.p_8, \\
H_2 &= p_1.p_3.p_4.p_5.p_6.p_7.p_8, \\
H_3 &= p_1.p_2.p_4.p_5.p_6.p_7.p_8, \\
H_4 &= p_1.p_2.p_3.p_5.p_6.p_7.p_8, \\
H_5 &= p_1.p_2.p_3.p_4.p_6.p_7.p_8, \\
H_6 &= p_1.p_2.p_3.p_4.p_5.p_7.p_8, \\
H_7 &= p_1.p_2.p_3.p_4.p_5.p_6.p_8, \\
H_8 &= p_1.p_2.p_3.p_4.p_5.p_6.p_7 \ ,
\end{aligned}
\tag{10}
$$

they represent weights that participate in the interpolation process. The property in the Chimera boundary point is therefore defined as

$$
P_f = \left(\frac{1}{\sum_{j=1}^{8} H_j} \right) \left(\sum_{i=1}^{8} Pv_i H_i \right), \tag{11}
$$

where Pv_i represents the values of the properties in the vertices that contribute to the interpolation of the properties of that particular point. In other words, they are the values of the properties in the eight vertices of a certain hexahedron of the mesh in which the Chimera boundary point is contained.

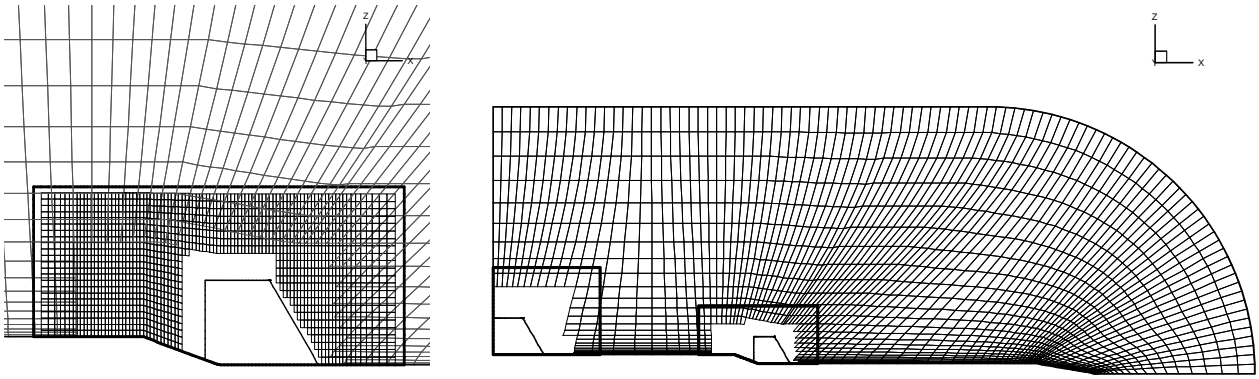

Figure 9. Detail of the “background” m_8 mesh (left) and central body m_{13} mesh (right) after the “holecutting” process.

7 Results and Discussion

The results presented refer to simulations of the flow over the SONDA-III rocket during its first stage flight. The specifc results included here consider only the case with freestream Mach number $M_\infty = 2.0$ and zero angle of attack, which is representative of the simulations performed so far for the configuration. Moreover, as the flight time in the lower atmosphere for these rockets is very short and the vehicle is at supersonic speeds during most of this flight, it seems appropriate to select a supersonic flight condition for the present discussion. Furthermore, the purpose of the present paper lies mostly in the capability implemented instead than a detailed account of the SONDA-III aerodynamics. Within the supersonic speed regime, several interesting aspects of the Chimera and patched grid techniques can be analyzed, such as the communication of information across the internal boundaries among blocks with discontinuities in the flow properties. As previously mentioned, the major interest in this work concerns the evaluation of the joint use of the Chimera and patched grid techniques as a tool for flow analysis on geometries of interest for the group.

As one can observe in Figs. (4) and (5), the afterbody portion of the vehicle has been simplified for the simulations here reported. This simplification has been performed because previus experience (Azevedo *et al.*, 1997; Strauss *et al.*, 1999) with afterbody flows has demonstrated the need for a viscous turbulent formulation for the adequate description of such flows. In the future, an accurate description of the aferbody will be included in the vehicle model, but this is beyond the scope of the present effort. Furthermore, the added complexity in the afterbody region would not contribute to the major interest of the present work.

Figure (10) exhibits the residue history for all the meshes. The CFL used was 0.9 and approximately 8000 iterations were needed to reach machine zero. Mach number contours for the central body, the front and back fins can be observed in Figs. (11) and (12), respectively. In these figures, the points which were eliminated from the holecutting process were not plotted. Figure (13) exhibits the recirculation zone that is formed in the trailing edge of the front fin. The main objective of this work was not to capture phenomena with that level of detail, but even so, in spite of the low resolution of the mesh in that area, the results were quite satisfactory.

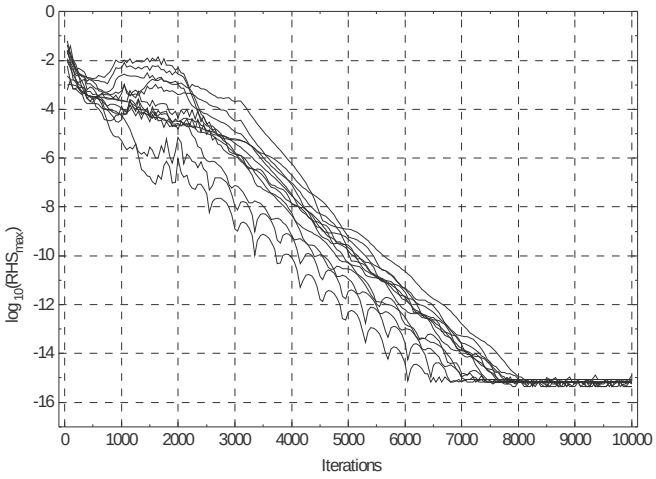

Figure 10. Residue history for all the meshes used in the simulation ($M_\infty = 2.0$ and CFL=0.9).

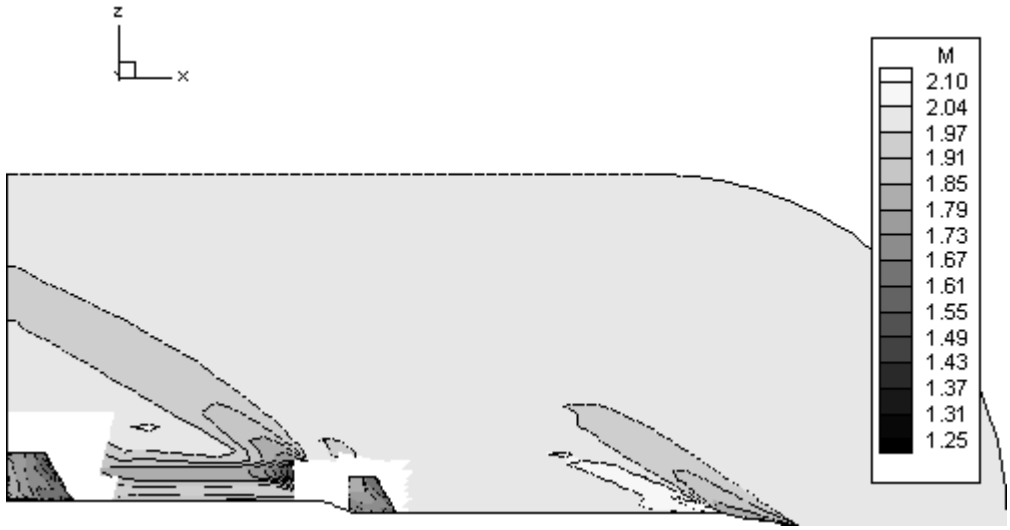

Figure 11. Mach number contours along the SONDA-III central body ($M_\infty = 2.0$ and α =0 deg.).

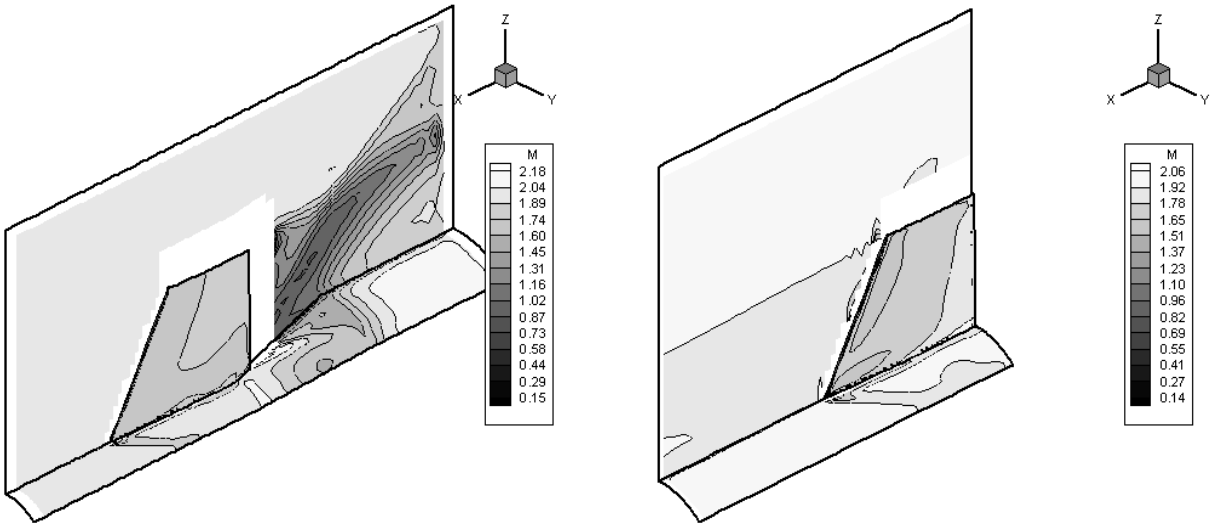

Figure 12. Mach number contours along the front and back fins ($M_\infty = 2.0$ and α =0 deg.).

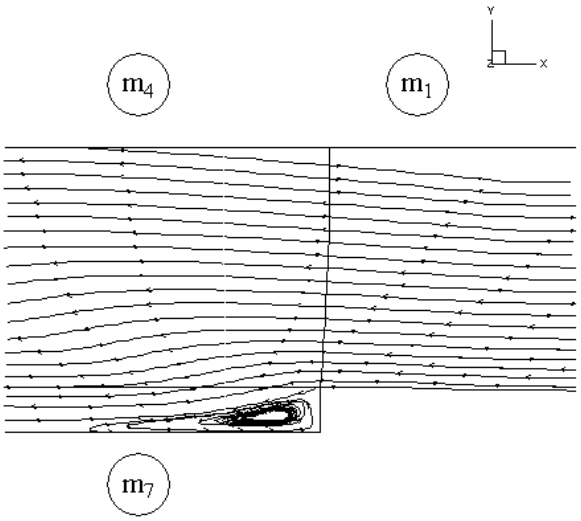

Figure 13. Recirculation zone in the front fin ($M_\infty = 2.0$ and α =0 deg.).

8 Concluding Remarks

The paper has presented results for 3-D Euler simulations of the flow over the SONDA-III, a typical sounding rocket. To the authors knowledge, this is the first time that such accurate and detailed simulation for the flow over the SONDA-III is performed and presented. A structured multiblock code has been implemented, using a Chimera and patched approach for handling the geometric complexity of the configuration. That was the first time that the group simulated a vehicle with fins and also a configuration in which there were body intersections (the central body with the fins, Figs. (1) and (2)). In spite of not having experimental results for comparison, the results here presented seem coherent. All codes used were developed by the research group and represent a powerful aerodynamic analysis and design tool. Finally, the presented methodology, using a combination of Chimera and patched approaches, seems to be convenient to work on similar problems with the presence of several fins. The main noteworthy advantages were:

- Flexibility: the use of Chimera and patched grids together allows the generation of meshes with much more ease and speed.
- Modularity: the use of "background" meshes allows hiding the complexity of the meshes that involve the fins. Small modifications are simple, because there is no need to generate all the meshes or even to reschedule the flow of information.
- Point concentration: the use of multiblock meshes allowed the refinement of localized areas in a way very similar to what can be achieved with the unstructured meshes.

The power of this combined Chimera/patched grid simulation capability becomes evident when one considers that it was possible to simulate the flow over a complete 8.7m long vehicle and, at the same time, to capture details of phenomena occurring along the trailing edge of the frontal fins, which have only 1.5cm semi-height. Furthermore, this was accomplished with a computational mesh of fairly modest size.

9 Acknowledgments

The authors acknowledge the partial support of Conselho Nacional de Desenvolvimento Científico e Tecnológico, CNPq, through the Integrated Project Research Grant No. 522413/96-0.

10 References

Azevedo, J.L.F., Menezes, J.C.L, and Fico, N.G.C.R., Jr., 1995, “An Assessment of Boundary Layer Properties for Transonic and Supersonic Flows over the VLS”, AIAA Paper No. 95-1769-CP, Proceedings of the 13th AIAA Applied Aerodynamics Conference, Part 1, San Diego, CA, pp. 41-51.

Azevedo, J.L.F., Menezes, J.C.L, and Fico, N.G.C.R., Jr., 1996, “Accurate Turbulent Calculations of Transonic Launch Vehicle Flows”, AIAA Paper No. 96-2484-CP, Proceedings of the 14th AIAA Applied Aerodynamics Conference, Part 2, New Orleans, LA, pp. 841-851.

Azevedo, J.L.F., Strauss, D., and Ferrari, M.A.S., 1997, “Viscous Multiblock Simulations of Axisymetric Launch Vehicle Flows”, AIAA Paper No. 97-2300-CP, Proceedings of the 15th AIAA Applied Aerodynamics Conference, Part 2, Atlanta, GA, pp. 664-674.

Basso, E., Antunes, A.P., and Azevedo, J.L.F., 2000, “Three Dimensional Flow Simulations Over a Complete Satellite Launcher with a Cluster Configuration”, Proceedings of the 18th AIAA Applied Aerodynamics Conference, Denver, CO.

Fletcher, C.A.J., 1988, “Computacional Techniques for Fluid Dynamics”, Vol. II, Spring-Verlag, New York, 484p.

Jameson, A., and Mavriplis, D., 1986, “Finite Volume Solution of the Two-Dimensional Euler Equations on a Regular Triangular Mesh”, AIAA Journal, Vol. 24, No. 4, pp. 611-618.

Jameson, A., Schmidt, W., and Turkel, E., 1981, “Numerical Solutions of the Euler Equations by Finite Volume Methods Using Runge-Kutta Time-Stepping Schemes”, AIAA Paper No. 81-1259.

Pulliam, T.H., and Steger, J.L., 1980, “Implicit Finite-Difference Simulations of Three-Dimensional Compressible Flow”, AIAA Journal, Vol. 18, No. 2, pp. 159-167.

Strauss, D., and Azevedo, J.L.F., 1999, “A Numerical Study of Turbulent Afterbody Flows Including a Propulsive Jet”, AIAA Paper No. 99-3190-CP, Proceedings of the 17th AIAA Applied Aerodynamics Conference, Norfolk, VA, pp. 654-664.

Turkel, E., and Vatsa, V.N., 1994, “Effect of Artificial Viscosity on Three-Dimensional Flow Solutions”, AIAA Journal, Vol. 32, No. 1, pp. 39-45.

Vieira, R., Azevedo, J.L.F., Fico, N.G.C.R., Jr., and Basso, E., 1998, “Three Dimensional Flow Simulation in the Test Section of a Slotted Transonic Wind Tunnel”, ICAS Paper No. 98-R.3.11, Proceedings of the 21st Congress of the International Council of the Aeronautical Sciences, Melbourne, Australia.